A Hybrid Switched Capacitor Converter Enabling Capacitive-Based Wireless Power Transfer for Battery Charging Applications

Jade Sund, Student Member, IEEE, and Samantha Coday, Member, IEEE

Department of Electrical Engineering and Computer Science, Massachusetts Institute of Technology

Email: jcsund@mit.edu

Abstract—This work investigates the feasibility of employing hybrid switched capacitor converters in wireless battery charging applications. A capacitively-isolated hybrid Dickson converter designed for use in low-power volume-constrained wireless power transfer applications is presented. The converter analysis, operation and design are detailed. Finally, a hardware prototype is presented and experimental results validate wireless power transfer, across varying load and gap distances.

Index Terms—hybrid switched capacitor converter, wireless power transfer, Dickson converter, resonant converter

I. Introduction

Wireless power transfer (WPT) is emerging for applications such as autonomous drones, electric vehicles, biomedical implants, and phone charging, where wired charging is inconvenient or impractical. Moreover, wired connections endure additional stresses on chargers, requiring user intervention and increasing failure rates. Inductive WPT (I-WPT), which utilizes magnetic coupling for power transfer, is dominant in on-market WPT solutions, with demonstration in industry [1] and academia [2] reaching high power density and efficiency. However, I-WPT systems suffer from high cost and rely on ferrite cores that are both fragile and heavy [3]. Demonstrations of I-WPT also face challenges in volume-constrained applications, as magnetics' sizing is limited by losses [4]. As such, capacitive WPT (C-WPT), which utilizes electric fields for power transfer, has been investigated as an alternative to I-WPT, in biomedical [2], electric vehicle [5], and autonomous underwater vehicles (AUV) [6] [7] charging applications. Previous research has focused on converter topologies composed of a dc source, inverter stage, resonant tank with capacitive coupling, rectifier stage, and load. These converter topologies are operated at high resonant frequencies (>1 MHz) to minimize the required capacitance and inductance. In high power (>1 kW) large air-gap applications, such as electric vehicle charging, this approach has achieved efficiencies of over 90% and power densities of over 49 kW/m² [5], [8]. In applications such as biomedical devices and underwater charging, the gap between plates is comprised of human tissue or water, both of which increase the dielectric constant by a factor of ten. However, these applications are extremely volume-constrained and previous demonstrations are limited in efficiency (< 40%) [2], [9], [10].

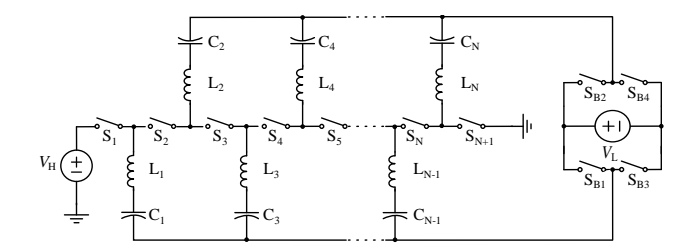


Fig. 1. Capacitively-isolated N:1 hybrid Dickson converter schematic.

As a result, this work investigates alternative topologies which increase effective capacitance and decrease inductor requirements. Hybrid switched capacitor converters have been shown to have high power density and efficiency due to their use of energy dense capacitors and low switch stress [11], [12]. The Dickson converter, a type of switched capacitor converter, was developed for on-chip energy processing [13], and has become a popular candidate for power dense conversion due to its low switch stress compared to other hybrid switched capacitor converters [14]. Previous work [15] [16] originally presented a modified hybrid Dickson converter which utilizes the flying capacitors to process energy and provide dielectric isolation. Here utilizing the capacitively-isolated hybrid Dickson topology for use in WPT systems, to decrease passive component sizing and switch stress is explored. The remainder of this work presents the analysis of the capacitively-isolated Dickson converter and results for both the 12:1 and 4:1 converters demonstrating its viability as a WPT solution.

II. THEORETICAL ANALYSIS

A. Converter Operation

The capacitively-isolated Dickson converter, shown as an N:1 converter in Fig. 1, where N is the converter level count and conversion ratio, can be operated bidirectionally; therefore, the voltage sources will be referred to as the high-side (V_H) and low-side (V_L) voltages. The capacitively-isolated Dickson converter can be operated as a two phase 50% switching scheme while maintaining soft-charging of the capacitors. In phase one, the odd numbered string switches, S_{B2} , and S_{B3} are closed and the remaining switches are open. In phase two, the even numbered switches, S_{B1} , and S_{B4} are

© 2025 IEEE. Personal use of this material is permitted. Permission from IEEE must be obtained for all other uses, in any current or future media, including reprinting/republishing this material for advertising or promotional purposes, creating new collective works, for resale or redistribution to servers or lists, or reuse of any copyrighted component of this work in other works.

DOI: 10.1109/APEC48143.2025.10977546

closed and the remaining switches are open. The drain-to-source blocking voltage of the switches are expressed in (1).

$$v_{ds,n} = \begin{cases} V_L & \text{for } n = 1, \ N+1 \\ 2V_L & \text{for } n = [2...N] \\ V_L & \text{for } B1 - B4 \end{cases}$$
 (1)

When the capacitor and inductor values are matched, e.g $C_1 = C_2 = \cdots = C_N \triangleq C$ and $L_1 = L_2 = \cdots = L_N \triangleq L$, the resonant frequency of the converter is as expressed in (2).

$$f_{res} = \frac{1}{2\pi\sqrt{IC}} \tag{2}$$

The capacitively-isolated Dickson converter is operated at resonance; therefore, the inductor sizing depends on the chosen switching frequency and the size of capacitive coupling shown in (3).

$$L = \frac{1}{(2\pi f_{res})^2 C}$$
 (3)

Moreover, like other resonant tank converters the capacitor ripple does not increase switch stress, allowing for sizing of switches independent of load and capacitance. The decreased switch stress also allows for the use of lower voltage switches, which have improved figures-of-merit [17]–[19].

The mid-range voltage analysis of the coupling capacitors results in (4) where V_{ISO} is the voltage difference between the ground of V_H and that of V_L and k is the index of the flying capacitor capacitor as seen in Fig. 1. In the capacitively-isolated Dickson converter, the energy processing capacitors $C_1 - C_N$, also provide isolation [16].

$$V_{C,k} = V_{ISO} + (N - k) V_L \tag{4}$$

There are multiple methods to achieve soft charging in the capacitively-isolated Dickson converter [20]; the method of distributed inductance, shown in Fig. 1, pairs each capacitor with a series inductor. The lumped inductance approach places an inductor at each of the rectifier switch nodes. While lumped inductance takes advantage of the fact that larger volume inductors have higher power density and efficiency [4], a distributed inductance approach was chosen to minimize the component volume on the receiving side of the converter. The component volume of the receive (RX) side is prioritized as in the applications of focus, AUV and biomedical charging, the RX volume is more critically constrained than the transmit (TX) volume.

B. Power Transfer Analysis

Power transfer analysis, following the method presented in [21], can be used to compare the maximum power transfer capabilities per gap distance of WPT topologies. This method requires the elimination of switching devices in the converter topology, which motivates the development of an ac equivalent circuit model for the N:1 capacitively-isolated Dickson converter. The model maintains the voltage characteristics of the LC tanks. The resultant model consists of replacing the string switches (S_2-S_{N+1}) with voltage sources whose values

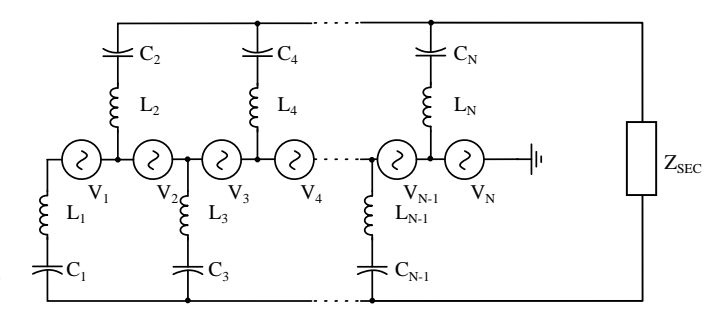


Fig. 2. Derived ac equivalent model for N:1 capacitively-isolated Dickson converter

are the sum of the mid-range voltage experienced by capacitor (k) and the ac voltage ripple across capacitor, as seen in (5). The two phase operation of the converter results in the even and odd capacitors having a phase shift of 180 degrees.

$$V_k = V_{dc_k} + v_{ac_k}$$

= $V_{C_k} + 2(-1)^k cos(\omega t + \phi)$ (5)

A load impedance, Z_{SEC} , replaces rectifier and secondary side passives [21]. The full model is presented in Fig. 2. The current delivered to the secondary by each voltage source is seen in (6), where C_T is the total coupling capacitance and $v_T(s)$ is the voltage across C_T where s is the complex frequency variable.

$$i_k(s) = \begin{cases} sC_T v_T(s) & k \text{ is even} \\ 0 & k \text{ is odd} \end{cases}$$
 (6)

The total current delivered to the load is seen in (7), indicating that the total power delivered is as expressed in (8).

$$i_T = \frac{sN}{2}C_T v_T(s) \tag{7}$$

$$P_L(s) = \left[\frac{sN}{2}C_T v_T\right]^2 Z_{SEC} \tag{8}$$

When the coupling capacitor values are matched, e.g $C_1 = C_2 = \cdots = C_N \triangleq C$, (8) can be expressed in terms of the total capacitive area (A), the relative permeability, (ε) , and the electric field strength of C_T where $C_T = \frac{N}{4}C$, (E(s)) as seen in (9).

$$P_L(s) = \left[\frac{sN}{g} A \varepsilon E(s)\right]^2 Z_{SEC} \tag{9}$$

In terms of the plate separation distance (d) and the ac voltage across the plates $(v_{ac}(s))$, (9) can be expressed as (10).

$$P_L(s) = \left[\frac{sN}{8} A \varepsilon \frac{v_{ac}(s)}{d}\right]^2 Z_{SEC}$$
 (10)

Assuming a purely resistive secondary impedance (9) can be expressed in the time domain as (11).

$$P_L(t) = \left[\frac{\omega N}{8} A \varepsilon E(t)\right]^2 R_{SEC} \tag{11}$$

$$= \left[\frac{\pi f_{sw} N}{4} A \varepsilon E(t)\right]^2 R_{SEC} \tag{12}$$

The 4:1 capacitively-isolated Dickson converter has the same

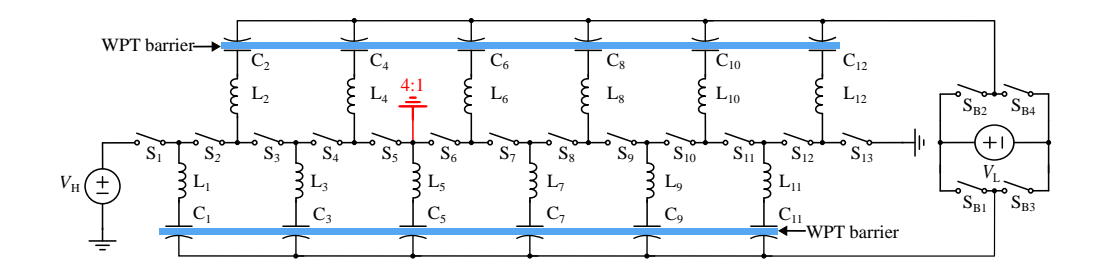


Fig. 3. Capacitively-isolated 12:1 hybrid Dickson converter schematic with WPT barrier shown. The ground connection (red) at the node between S_5 and S_6 converts the schematic to the 4:1 capacitively-isolated hybrid Dickson converter when $S_6 - S_{13}$, $L_5 - L_{12}$, and $C_5 - C_{12}$ are omitted.

power transfer capabilities as conventional C-WPT topologies, such as the resonant capacitor converter [21]. Moreover, unlike the conventional approaches, the proposed converter provides a N:1 voltage conversion. This conversion provides an interesting system benefit in many applications, such as biomedical devices charging, where a step down stage is necessary and usually employed with an additional converter. Furthermore, (11) suggests that the power transfer capabilities of the capacitively-isolated Dickson converter with N > 4 exceed those of conventional C-WPT approaches. The N dependence of (11) indicates that there is a nine-fold improvement in power transfer capabilities of the 12:1 capacitively-isolated Dickson converter over the 4:1 capacitive-isolated and 1:1 conventional C-WPT topologies with the same operating conditions. However, this conversion may not be preferable in many other applications which require 1:1 voltage; therefore, requiring further system level optimization depending on application space.

C. Passive Component Selection

The capacitors, $C_1 - C_N$, are realized through aligning exposed copper platting, seen coated in Kapton tape in Fig. 4b, on the TX and RX printed circuit boards (PCBs). Kapton tape has a similar dielectric to coatings commonly used for bio-compatibility and corrosion prevention in biomedical and AUV applications. The capacitance, seen in (13), is determined by the plate area (A), distance between plates (d_1), dielectric constant of WPT medium (ε_1), thickness of coating (d_2), and dielectric constant of coating (ε_2).

$$C = \frac{A\varepsilon_1 \varepsilon_2}{d_1 \varepsilon_2 + d_2 \varepsilon_1} \tag{13}$$

The plate area, distance between plates, and dielectric constant of the medium are fixed by the application; the choice and thickness of the coating can be used to control the final capacitance. In conditions where $d_2\varepsilon_1 >> d_1\varepsilon_2$, the capacitance equation simplifies to (14).

$$C = \frac{A\varepsilon_2}{d_2} \tag{14}$$

III. HARDWARE

To validate the analysis presented in Section II, a hardware prototype of the capacitively-isolated Dickson converter which can be operated at either a 4:1 or 12:1 conversion ratio was developed.

For the initial hardware prototype the capacitance was estimated using (13) to be 1.01 nF when coated with 1 mil thick Kapton tape. As a trade-off in inductor sizing and switching losses, and initial switching frequency of 100 kHz was selected, resulting in a designed inductance of 2.5 mH. With the increased number of coupling capacitors, the parasitic capacitance between the plates becomes a larger challenge for design and analysis. As described in [22], parasitic capacitance is important to characterize for optimal performance in C-WPT systems. Parasitic capacitance can lead to decreased output power and is a focus of future work.

Components	Part Number	Description
S_1 - S_{13} , S_{B1} - S_{B4}	GSF3404B	30 V, 43 mΩ
L_1 - L_{12}	SDS680R	2.2 μH, 0.1 A
Gate Driver	NCP81074	5 V, 10 A
Signal Isolator	ADUM5241	Power and Signal

TABLE I

COMPONENTS SELECTED FOR CAPACITIVELY-ISOLATED DICKSON CONVERTER HARDWARE PROTOTYPE.

The components for the prototype are listed in Table I. This initial prototype uses an ADUM for power and signal isolation but bootstrapping methods can be implemented to improve end-to-end efficiency [23], [24].

Two PCBs were designed to realize the converter of Fig. 3; each PCB represents one side of the WPT barrier seen in Fig. 3. The TX PCB is designed such that one side of the board contains the string switches (S_1 - S_{13}), the gate drive for the string switches, the inductors (L_1 - L_{12}), and all control circuitry as seen in Fig. 4a and Fig. 5a. The other side of the board contains only the TX plate for the capacitors C_1 - C_{12} , whose layout is identical to the that shown in Fig. 4b. When operated as a 4:1 converter, a connection to ground is made, shown in red in Fig. 3, and the rest of the string switches ($S_6 - S_{13}$) and inductors ($L_5 - L_{12}$) are

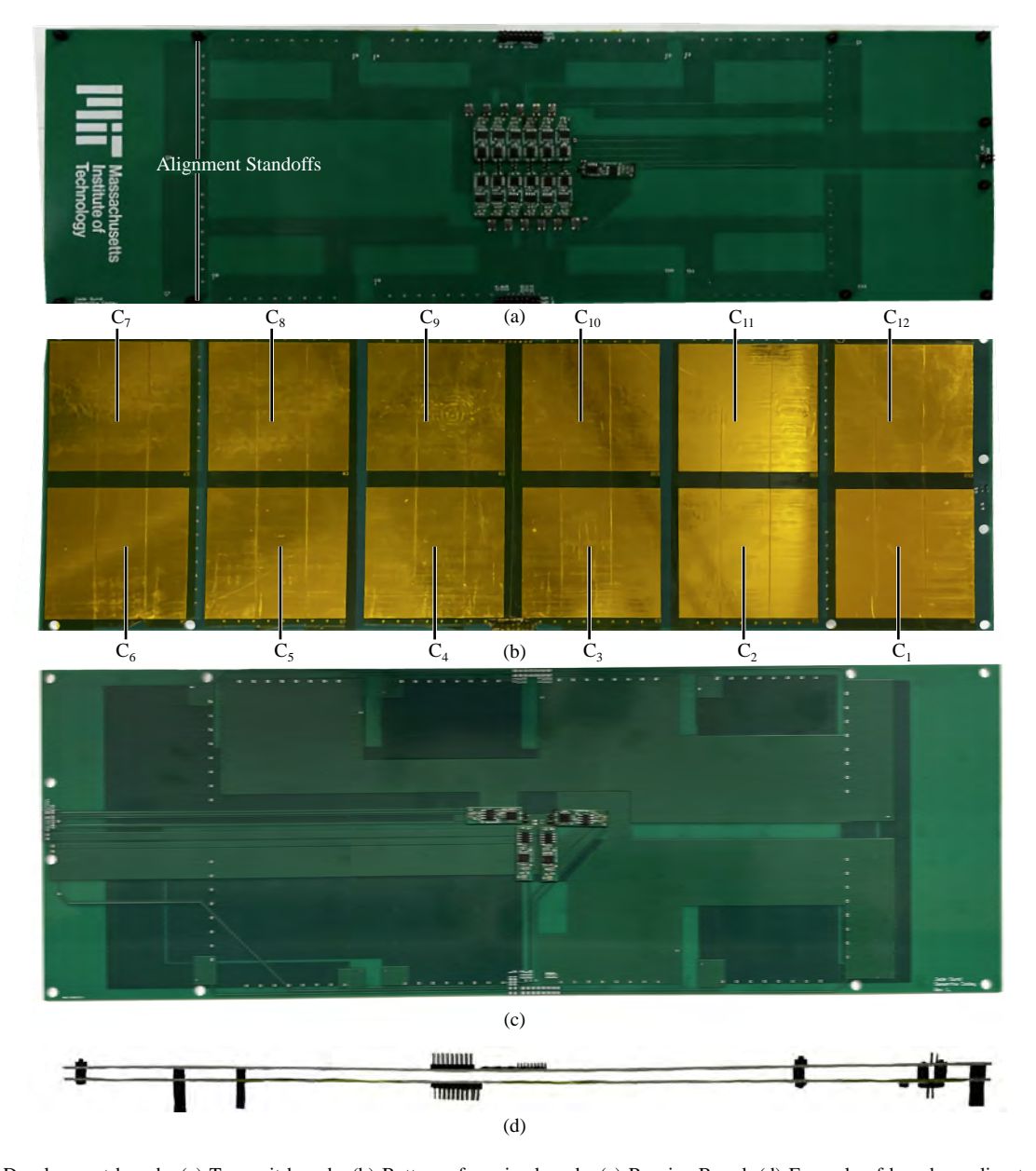


Fig. 4. Development boards. (a) Transmit boards. (b) Bottom of receive boards. (c) Receive Board. (d) Example of board coupling technique.

not populated. The RX PCB represents the low-side of the WPT barrier; the RX board is designed such that one side of the board contains the rectifier shown in Fig. 5b and the other contains the receive plate for capacitors C_1 - C_{12} . The two PCBs are coupled though the capacitive plates of the TX and RX boards. De-ionized water was selected for the dielectric, as the dielectric constant is similar to that of undersea AUV and biomedical charging, where the anticipated dielectric constants are ≈ 69 and 30-80, respectively. For this preliminary prototype, proper alignment and spacing of the capacitive plates is achieved through standoffs placed along the edges of the board as seen in Fig. 4d.

A. Board Design

Minimizing commutation loop area and thereby parasitic inductance is paramount for ensuring low voltage overshoot, noise, and EMI, allowing for higher switching frequency operating and efficiency. In particular, due to the high number of switches and the comparatively large capacitors, the design of the Dickson converters' commutation loop is challenging. Here, seen in Fig. 5a, switches S_1 - S_{13} are placed in a rectangular shape on the board to reduce the distance between the drain and source of adjacent switches. Further reduction in the drain-to-source distance is limited by the associated loss of symmetry, which is utilized to minimize parasitic mismatch.

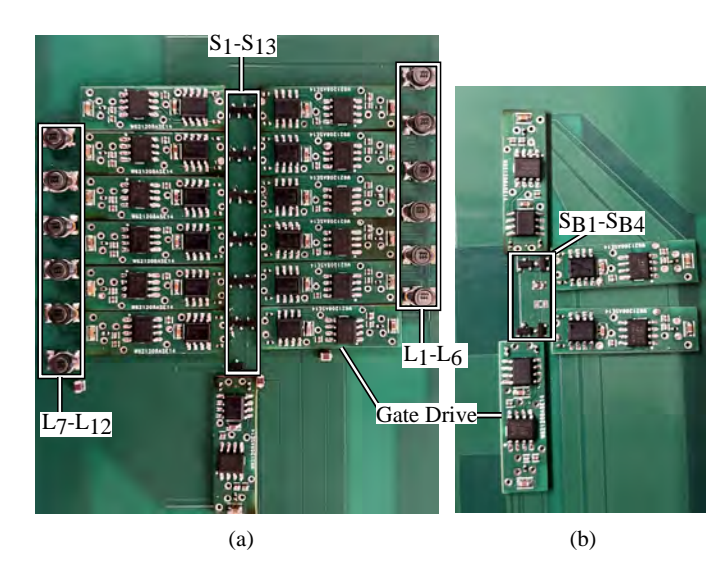


Fig. 5. Development boards. (a) Transmit board switching cells. (b) Receive board switching cell.

IV. RESULTS

The 12:1 isolated Dickson converter was tested at $V_H = 48$ V, switching frequency of 42.5 kHz and a dielectric of de-ionized water. The 4:1 isolated Dickson converter was tested at $V_H = 16$ V, switching frequency of 75 kHz, and a dielectric of de-ionized water. The output voltage of both converters with no loss is expected to be $V_L = 4$ V.

A. Resonant Frequency Tuning

For full soft charging of capacitors and thus maximum output power the converter needs to be operated at resonance. In the ideal case where the capacitors and inductors are perfectly matched, e.g $C_1 = C_2 = \cdots = C_N \triangleq C$ and $L_1 = L_2 = \cdots = L_N \triangleq L$, the capacitor voltage waveforms should be sinusoidal. The sinusoidal nature of a waveform was determined by comparing the RMS measured by the oscilloscope and the RMS calculated using the measured amplitude of the waveform. When the capacitor voltages are sinusoidal there should be little mismatch between these two values. The frequency that results in the minimum mismatch was determined to be the resonant frequency. Furthermore, the resonant frequency, calculated in this manner, should be the same for all capacitor voltages.

For the 4:1 capacitively-isolated Dickson converter, the frequency that minimizes the difference in measured RMS and calculated RMS for V_{C1} results in a resonant frequency of 88.9 kHz, shown in Fig. 6a. The output voltage, at this frequency is 0.29 V with $V_H = 12$ V and 6 k Ω load.

The desired operation frequency can also be determined by finding the frequency that maximizes the output voltage. The resultant capacitor voltage waveforms for operation of the 4:1 isolated Dickson converter at 75 kHz, the frequency that maximizes output voltage, are shown in Fig. 6b At this operation frequency, with a 6 k Ω load, the output voltage is

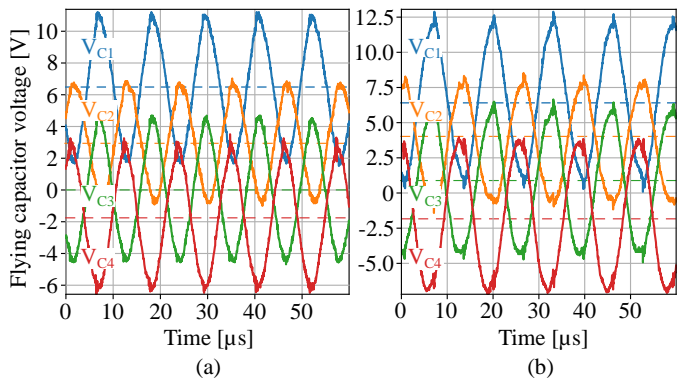


Fig. 6. 4:1 capacitively-isolated Dickson converter capacitor voltages with $V_H = 12$ V. (a) $f_{sw} = 88.9$ kHz. (b) $f_{sw} = 75$ kHz.

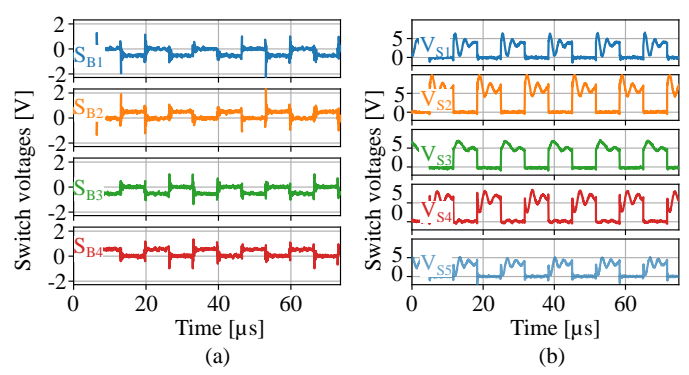


Fig. 7. 4:1 isolated Dickson converter switch waveforms for $V_H = 12$ V, $V_L = 0.31$ V. (a) RX bridge switches reference to input ground. (b) TX string switches.

0.58 V with $V_H = 12$ V. Note that the voltage ripple on C_1 is larger in Fig. 6b than Fig. 6a. In contrast, there is a larger discontinuity at the peaks and troughs of V_{C1} in Fig. 6b than Fig. 6a. In the case where operation frequency is determined by output voltage, the smoothness of the voltage waveform is traded for and increased waveform amplitude. The resonant frequency, 88.9 kHz in the case of the 4:1 isolated Dickson converter, is used to calculate the coupling capacitance of $C_1 = 3.2$ nF. This is significantly larger than the theoretical value calculated from (13), which implies the presence of large parasitic capacitance.

B. Switch Voltages

As discussed in Section III, minimizing the commutation loop is important in reducing voltage overshoot at the switch nodes. Figure 7b shows the voltages across S_1 - S_5 for the 4:1 converter operated at $V_H = 16$ V. The ripple seen on these switch voltages is a function of the capacitor mismatch as well as the commutation loop inductance. Further design to minimize the commutation loop may decrease the ripple seen here. The voltage across the bridge switches, shown in Fig. 7a, indicates that the rectifier switches are functioning as expected.

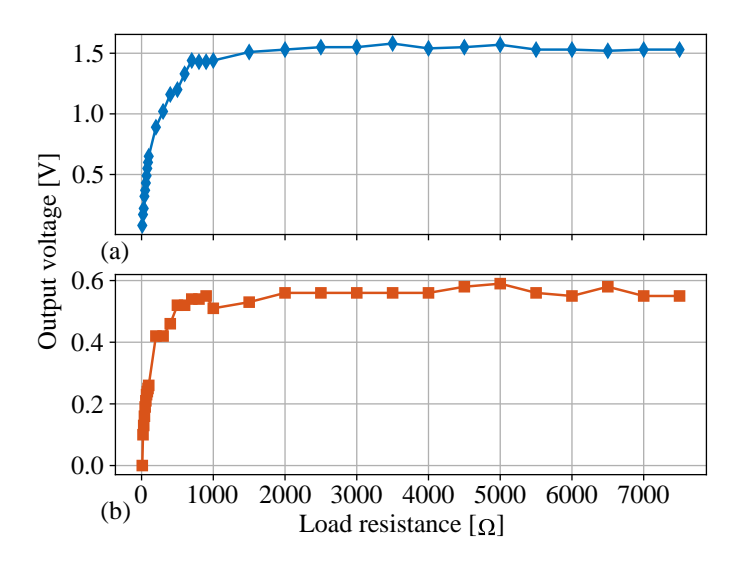


Fig. 8. Load resistance versus output voltage for (a) 12:1 capacitively-isolated Dickson converter operated at $V_H = 48$ V and $f_{sw} = 46.5$ kHz and (b) 4:1 capacitively-isolated Dickson converter operated at $V_H = 16$ V and $f_{sw} = 75$ kHz.

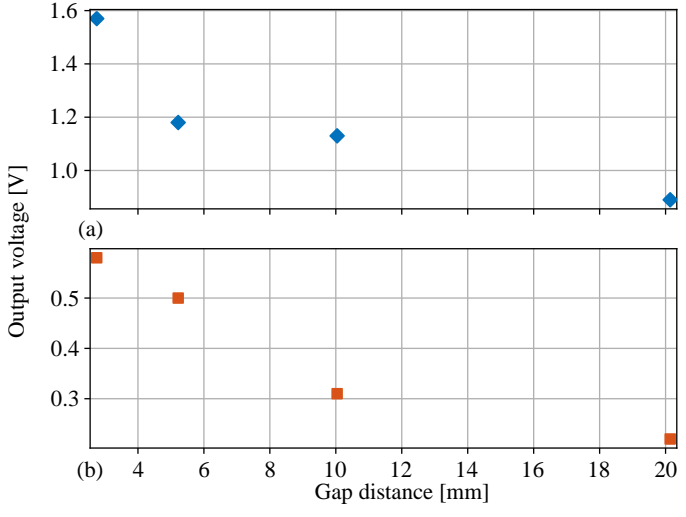


Fig. 9. Output voltage as a function of gap distance (d_2) for (a) 12:1 capacitively-isolated Dickson converter operated at $V_H=48$ V, $f_{sw}=46.5$ kHz and 6 k Ω load and (b) 4:1 capacitively-isolated Dickson converter operated at $V_H=16$ V, $f_{sw}=75$ kHz and 6 k Ω load.

C. Capacitor Voltages

The sinusoidal nature of the capacitor voltages, in Fig. 6a, indicates coupling between the TX and RX board capacitor plates was achieved and the converter is operating at resonance with minimal hard charging of the capacitors. Compared to the analysis in Section II-A, the experimental capacitor waveforms have variable amplitudes and phase shifts. Furthermore, the 12:1 converter voltage waveforms shows increased capacitor mismatch when compared to the 4:1 converter. The variations in amplitude and phase are likely due to parasitic capacitance throughout the converter. Techniques to minimize and mitigate the effects of parasitic capacitance need to be investigated. The value of the series inductance can be independently tuned to allow for equivalent resonant frequencies across LC tanks with variable capacitance to mitigate the effect of capacitor mismatch.

D. Output

The output voltages of the 4:1 and 12:1 capacitively-isolated Dickson converters are shown in Fig. 8 as a function of load and in Fig. 9 as a function of gap distance. The output voltage of the 4:1 remains constant over a wide range of load resistances. The output voltage decays as a function of gap distance.

CONCLUSION

This work presents a hybrid switched capacitor approach to capacitive wireless power transfer in battery charging applications. The analysis and design of an capacitively-isolated Dickson converter is considered. A hardware prototype is presented which validates the capacitively-isolated Dickson converter's ability to transfer power wirelessly.

REFERENCES

- A. Kurs and G. Lestoquoy, "A framework for evaluating multi-kilowatt highly-resonant wireless power transfer systems," 2015 IEEE 82nd Vehicular Technology Conference (VTC2015-Fall), pp. 1–6, 2015.
- [2] R. Erfani, F. Marefat, A. M. Sodagar, and P. Mohseni, "Transcutaneous capacitive wireless power transfer (c-wpt) for biomedical implants," *IEEE International Symposium on Circuits and Systems (ISCAS)*, pp. 1– 4, May 2017.
- [3] G. A. Covic and T. Boys, J, "Modern trends in inductive power transfer for transportation applications," *IEEE Journal of Emerging and Selected Topics in Power Electronics (JESTPE)*, vol. 1, pp. 28–41, Mar. 2013.
- [4] C. Sullivan, B. A. Reese, A. L. F. Stein, and K. P. A., "On size and magnetics: Why small efficient power inductors are rare," 2016 International Symposium on 3D Power Electronics Integration and Manufacturing (3D-PEIM), pp. 1–23, 2016.
- [5] F. Lu, H. Zhang, H. Hofmann, and C. Mi, "A double-sided lclc-compensated capacitive power transfer system for electric vehicle charging," *IEEE Transactions on Power Electronics*, vol. 30, pp. 6011 14, Nov. 2015.
- [6] L. Yang, L. Ma, J. Huang, and Y. Fu, "Characteristics of undersea capacitive wireless power transfer system," 2020 IEEE 9th International Power Electronics and Motion Control Conference (IPEMC2020-ECCE Asia), p. 2952–2955, Nov. 2020.
- [7] H. Li, G. Li, X. Jin, J. Li, and G. Xu, "A lc-cll compensated capacitive wireless power transfer system in fresh water," 5th International Conference on Power and Energy Applications (ICPEA), pp. 130–137, Nov. 2022
- [8] S. Regensburger, B. Sinha, A. Kumar, and K. K. Afridi, "A 3.75-kw high-power-transfer-density capacitive wireless charging system for evs utilizing toro idal-interleaved-foil coupled inductors," *IEEE Transporta*tion Electrification Conference and Expo (ITEC), p. 839–843, June 2020.
- [9] R. Erfani, F. Marefat, A. M. Sodagar, and P. Mohseni, "Modeling and experimental validation of a capacitive link for wireless power transfer to biomedical implants," *EEE Trans. Circuits Syst. II*, vol. 65, pp. 923– 927, July 2018.
- [10] A. Koruprolu, S. Nag, R. Erfani, and P. Mohseni, "Capacitive wireless power and data transfer for implantable medical devices," *IEEE Biomedical Circuits and Systems Conference (BioCAS)*, pp. 1–4, Oct. 2018.
- [11] Z. Ye, S. R. Sanders, and R. C. N. Pilawa-Podgurski, "Modeling and comparison of passive component volume of hybrid resonant switchedcapacitor converters," *IEEE Trans. Power Electron.*, vol. 37, pp. 10903– 10919, Sept. 2022.
- [12] N. M. Ellis, N. C. Brooks, M. E. Blackwell, R. A. Abramson, S. Coday, and R. C. N. Pilawa-Podgurski, "A general analysis of resonant switched

- capacitor converters using peak energy storage and switch stress including ripple," *IEEE Trans. Power Electron.*, pp. 1–21, 2023.
- [13] J. F. Dickson, "On-chip high-voltage generation in mnos integrated circuits using an improved voltage multiplier technique," *IEEE J. Solid-State Circuits*, vol. 11, pp. 374–378, June 1976.
- [14] R. C. N. Lei, Y. Pilawa-Podgurski, "A general method for analyzing resonant and soft-charging operation of switched-capacitor converters," *IEEE Transactions on Power Electronics*, vol. 30, no. 10, pp. 5650–5664, 2015.
- [15] A. Jackson, N. M. Ellis, and R. C. N. Pilawa-Podgurski, "A capacitivelyisolated dual extended lc-tank hybrid switched-capacitor converter," *IEEE Applied Power Electronics Conference and Exposition (APEC)*, vol. 15, pp. 1279 –1283, Mar. 2022.
- [16] S. Coday, E. Krause, M. E. Blackwell, N. M. Ellis, A. Barchowsky, and R. C. N. Pilawa-Podgurski, "Design and implementation of a gan-based capacitively-isolated hybrid dickson switched-capacitor dc-dc converter for space applications," 2023 IEEE Applied Power Electronics Conference and Exposition (APEC), pp. 3154–3159, 2023.
- [17] J. Stauth, "Pathways to mm-scale dc-dc converters: Trends opportunities and limitations," *Proc. IEEE Custom Integr. Circuits Conf. (CICC)*, pp. 1–8, 2018.
- [18] M. Guacci, D. Bortis, and J. W. Kolar, "High-efficiency weight-optimized fault-tolerant modular multi-cell three-phase gan inverter for next generation aerospace applications," 2018 IEEE Energy Conversion Congress and Exposition (ECCE), pp. 1334–1341, Sept. 2018.
- [19] R. A. Abramson, S. J. Gunter, D. M. Otten, K. K. Afridi, and D. J.

- Perreault, "Design and evaluation of a reconfigurable stacked active bridge dc/dc converter for efficient wide load-range operation," 2017 IEEE Applied Power Electronics Conference and Exposition (APEC), pp. 3391–3401, Mar. 2017.
- [20] P. H. McLaughlin, J. S. Rentmeister, M. H. Kiani, and J. T. Stauth, "Analysis and comparison of hybrid-resonant switched-capacitor dc-dc converters with passive component size constraints," *IEEE Trans. Power Electron.*, vol. 36, pp. 3111–3125, Mar. 2021.
- [21] S. Sinha, S. Maji, and K. K. Afridi, "Comparison of large air-gap inductive and capacitive wireless power transfer systems," *IEEE Applied Power Electronics Conference and Exposition (APEC)*, 2021.
- [22] S. Sinha, A. Kumar, B. Regensburger, and K. K. Afridi, "A new design approach to mitigating the effect of parasitics in capacitive wireless power transfer systems for electric vehicle charging," *IEEE Trans. Transp. Electrific.*, vol. 5, p. 1040–1059, Dec. 2019.
- [23] Z. Ye, Y. Lei, W. C. Liu, P. S. Shenoy, and R. C. N. Pilawa-Podgurski, "Improved bootstrap methods for powering floating gate drivers of flying capacitor multilevel converters and hybrid switched-capacitor converters," *IEEE Transactions on Power Electronics*, vol. 35, pp. 5965– 5977, June 2020.
- [24] R. K. Iyer, N. M. Ellis, Z. Ye, and R. C. N. Pilawa-Podgurski, "A high-efficiency charge-pump gate drive power delivery technique for flying capacitor multi-level converters with wide operating range," 2021 IEEE Energy Conversion Congress and Exposition (ECCE), pp. 5360–5365, 2021